

From micro to macroevolution: drivers of shape variation in an island radiation of *Podarcis* lizards

Maxime Taverne,^{1,2} Hugo Dutel,^{3,4} Michael Fagan,⁴ Anamaria Štambuk,⁵ Duje Lisičić,⁵ Zoran Tadić,⁵ Anne-Claire Fabre,⁶ and Anthony Herrel¹

¹UMR 7179, Département Adaptations du Vivant, Muséum National d'Histoire Naturelle, Centre National de la Recherche Scientifique, Paris, France

²E-mail: maxime.taverne@mnhn.fr

³School of Earth Sciences, University of Bristol, Bristol, UK

⁴Department of Engineering, Medical and Biological Engineering Research Group, University of Hull, Hull, UK

⁵Department of Biology, Faculty of Science, University of Zagreb, Zagreb, Croatia

⁶Department of Life Sciences, The Natural History Museum, London, UK

Received January 12, 2021

Accepted July 21, 2021

Phenotypic traits have been shown to evolve in response to variation in the environment. However, the evolutionary processes underlying the emergence of phenotypic diversity can typically only be understood at the population level. Consequently, how subtle phenotypic differences at the intraspecific level can give rise to larger-scale changes in performance and ecology remains poorly understood. We here tested for the covariation between ecology, bite force, jaw muscle architecture, and the three-dimensional shape of the cranium and mandible in 16 insular populations of the lizards *Podarcis melisellensis* and *P. sicula*. We then compared the patterns observed at the among-population level with those observed at the interspecific level. We found that three-dimensional head shape as well as jaw musculature evolve similarly under similar ecological circumstances. Depending on the type of food consumed or on the level of sexual competition, different muscle groups were more developed and appeared to underlie changes in cranium and mandible shape. Our findings show that the local selective regimes are primary drivers of phenotypic variation resulting in predictable patterns of form and function. Moreover, intraspecific patterns of variation were generally consistent with those at the interspecific level, suggesting that microevolutionary variation may translate into macroevolutionary patterns of ecomorphological diversity.

KEY WORDS: Bite force, diet, geometric morphometrics, head shape, intraspecific variation, island, lizards, sexual competition.

Any biological structure is the result of the interplay between the phylogenetic heritage of the organism, its function, and its development (Thompson 1942; Gould and Lewontin 1979; Goodwin and Trainor 1980; Pigliucci and Kaplan 2000). The morphology of an organism thus reflects the constraints imposed by the physical and biological characteristics of its environment (Sagnes et al. 1997; Fish 1998; Hedenström 2002; Fish et al. 2008; Altshuler et al. 2015; Hedenström and Johansson 2015; Segall et al.

2019) within the limits imposed by its genetic and developmental repertoire. Comparative studies have convincingly demonstrated that the evolution of phenotypic diversity occurs in response to the selective pressures imposed by different ecological contexts (e.g., Boag and Grant 1981; Losos 1990) or life-history strategies (Fabre et al. 2020, Fabre et al. 2021). However, functional and constructional trade-offs may limit or constrain the expression of a given phenotype (Cheverud 1982; Barel et al. 1989;

Herrel et al. 2009). Moreover, genetic architecture may drive the direction and magnitude of phenotypic change (Lande 1976), thus driving the evolution of traits along genetic lines of least resistance (Schluter 1996, 2000; McGlothlin et al. 2018). This concept has been extended to phenotypic traits (Marroig and Cheverud 2005; Renaud et al. 2011) suggesting that variation within and between populations is often aligned with selection acting on axes of variation most prominent within populations. Population-level studies are consequently particularly insightful in helping to understand the drivers of phenotypic variation because they can inform us on the processes driving variation in morphology (Stuart et al. 2014; Campbell-Staton et al. 2017; Donihue et al. 2018).

The skull has been studied extensively as it fulfills many essential tasks including feeding, the protection of the sensory organs and the brain, interactions with conspecifics or other species, and even locomotion in some taxa (Wake 2003; Herrel et al. 2007). Consequently, the skull of vertebrates likely evolves in response to a variety of factors including physical constraints (Roscito and Rodrigues 2010; Rodrigues et al. 2015; Da Silva et al. 2018; Segall et al. 2020), activity patterns (Martin and Ross 2005), and foraging strategies (Reilly et al. 2007). However, complex integrated systems such as the vertebrate feeding system are not mechanically optimized structures (Zweers 1979; Wake and Roth 1989), rendering inferences of function from form often difficult and complex. The skull is composed of multiple bones arranged to carry out the aforementioned functions, while providing attachment areas for the masticatory muscles, and resisting the external forces generated during a behavior. As bone is a living tissue that is remodeled by the magnitude and the direction of the forces it experiences (Currey 2002; Renaud et al. 2010), it can be expected that the shape of cranium and mandible are strongly integrated with jaw muscle architecture (Fabre et al. 2014a; Cornette et al. 2015; Fabre et al. 2018), masticatory function, and by inference, with the diet of an animal. For these reasons, the cranial shape can be expected to diverge quickly among populations that differ in local selective regimes. The skull thus represents a biological structure that is relevant to address questions on how microevolutionary processes drive changes in morphology that subsequently may translate into macroevolutionary patterns of phenotypic variation. Islands represent excellent study systems to address these questions as they are relatively simple and replicated ecosystems, allowing the drivers of variation in form and function to be teased apart (Losos 2009; Losos and Ricklefs 2009; Kueffer et al. 2014). Moreover, insular systems often impose strong ecological pressures, thus favoring the emergence of adaptive responses in morphology (Baeckens and Van Damme 2020).

A previous study (Taverne et al. 2019) highlighted natural variation in the diet and the ecology of insular populations of

Podarcis lizards living on small islands in the Adriatic. These populations range from insectivorous to omnivorous, with lizards relying on difficult to chew food items (i.e., plant material and hard prey) to face the food scarcity observed in the smallest and most depauperate environments. Additionally, a recent study demonstrated that the proportion of these mechanically resistant items in the diet as well as the level of sexual competition are important drivers of variation in bite force in these lizards (Taverne et al. 2020). Variation in bite force is partly driven by variation in head shape (Herrel et al. 2001, Herrel et al. 2010; Verwaijen et al. 2002; Lappin et al. 2006; Huyghe et al. 2009; Wittorski et al. 2016), as taller and wider heads provide more space for muscles (Herrel et al. 2007). However, relatively weak correlations between bite force and external head dimensions were detected in these insular *Podarcis* lizards (Taverne et al. 2020), suggesting that variation in bite force is probably driven more by variation in muscle architecture. Subtle morphological differences between populations underlying variation in muscle architecture are, however, likely not quantifiable through external and linear measurements (Fabre et al. 2014b; Lappin and Husak 2005). Three-dimensional geometric morphometrics (Bookstein, 1997; Klingenberg 2002, 2011; Gunz et al. 2005; Kaliontzopoulou 2011; Adams et al. 2013) represents a powerful alternative for quantifying morphological variation, and determining how it relates to variation in performance and diet. Despite the availability of this tool, surprisingly few studies have quantified intraspecific morphological variation in skull shape in association with variation in muscles and bite force (but see Fabre et al. 2014a; Herrel et al. 2007).

The Croatian archipelago of the Adriatic is the second largest archipelago in the Mediterranean, comprising almost 700 islands and islets. This archipelago provides a unique opportunity to study independent populations of two species of *Podarcis* lizards, *Podarcis melisellensis* and *Podarcis sicula*. The islands in this archipelago were separated at the end of the last glaciation (approximately 18,000 years ago), when sea levels rose. Given the presence of both species on multiple islands, this system permits us to explore whether intraspecific ecomorphological patterns are repeated at the interspecific level. To tackle this question, we carried out a comparative study including 139 specimens from 16 insular populations of the two *Podarcis* species. We first asked ourselves whether patterns of evolution in cranial morphology and anatomy occurring among populations are similar in similar ecological contexts. To do so, we used geometric morphometrics to test for the covariation between the shape of the skull and mandible in 3D, jaw musculature, bite force, and ecological variables.

We predict that variation in bite force and jaw musculature will co-vary with the type of food items consumed and with the level of sexual competition within the populations; that skull and

mandible shape will covary with muscle architecture and with ecological traits. We predict that these patterns would hold even when accounting for the phylogenetic relationships between populations, suggesting that the masticatory apparatus is independently evolving toward similar morphologies under comparable ecological circumstances. Additionally, we predict that the evolutionary trajectories within each species will be congruent with those among species. Specifically, we predict that the functional associations of the skull and diet will be similar irrespective of the species considered.

Material and Methods

SPECIMENS, ECOLOGICAL, AND BITE FORCE DATA

The 16 populations of interest were sampled across 14 islands in the Adriatic and two mainland sites. Adult lizards were captured by noose or by hand at the end of the summer of 2016. In total, 455 specimens were captured (Table S1). All individuals were stomach-flushed right after capture using a syringe with ball-tipped steel needle (Herrel et al. 2006). Stomach contents were preserved in individual vials containing a 70% aqueous ethanol solution and analyzed as described in Taverne et al. (2019). Briefly, we recorded the volumetric proportion of plants and hard arthropods consumed relative to the total volume of the bolus. Sexual dimorphism in head dimensions of each population was calculated. To do so, we measured head dimensions of every specimen, \log_{10} -transformed them, and calculated the mean distance between males and females along the first axes of a PCA. This measure of sexual dimorphism in head dimensions was previously demonstrated to be a good indicator for the level of sexual competition in these populations (Taverne et al. 2020). *In vivo* bite force was measured for all individuals as described in Taverne et al. (2020). To do so, we made lizards bite on the plates of a bite force setup containing an isometric Kistler force transducer (type 9203) connected to a Kistler charge amplifier (type 5995, Kistler Inc., Winterthur, Switzerland; see Herrel et al. 1999a for a detailed description of the set-up) while standardizing gape and bite point.

CT SCANNING

We sacrificed five male and five female lizards of each population, where authorized (see Table S1), by means of an intramuscular injection of pentobarbital. Lizards were fixed in a 10% aqueous formaldehyde solution for 48 h, rinsed, and transferred to a 70% ethanol solution. Specimens were scanned using an X-Tek HMX 160 μ CT system (Nikon, X-Tek Systems Ltd, UK) at a voxel size of 24.90 μ m with the following parameters: X-ray voltage, 90 kV; X-ray intensity, 70 μ A; exposure time, 2000 ms; number of projections, 2500. Scans were segmented using Avizo

9.0 (Thermo Fischer Scientific) and 3D surfaces of the cranium and mandible were reconstructed and exported separately.

GEOMETRIC MORPHOMETRICS

Anatomical landmarks were placed on the left side of the skull and mandible in Idav Landmark 3.6 (Institute for Data Analysis and Visualization, University of California, Davis). Each hemimandible was defined by 33 anatomical landmarks, and each half of the cranium by 47 landmarks (Table 1). In addition, 54 and 49 semi-landmarks on curves were digitized on the cranium and mandible, respectively (Figures 1, 2). The set of points was chosen to describe the whole three-dimensional structure, focusing on areas of muscle insertion (e.g., the quadrate, the lateral side of the mandible) and other areas potentially relevant from a mechanical perspective (e.g., the shape of the snout, the curvature of the mandible). Sliding semi-landmarks were projected onto the surface using a thin-plate spline deformation (Gunz and Mitteroecker 2013) and slid. Next, three iterations of thin-plate spline relaxation were performed against a Procrustes consensus, using the library “Morpho” (Schlager 2013). Anatomical landmarks and curves of the skull were mirrored across the sagittal plane (“mirrorfill” function from “paleomorph” package) (Cardini 2016; 2017).

MUSCULATURE

After scanning, cranial muscles were dissected on the left side of the skull of each specimen, blotted dry and weighed using a digital balance (Mettler AE100; ± 0.1 mg). Muscle volume was obtained by dividing muscle mass by density (1.06 g/cm³; Mendez et al. 1960). Muscles were immersed in an aqueous solution of nitric acid (30%) for 20 to 24 h to digest the connective tissues and to separate muscle fibers. Muscles were then transferred into a 50% aqueous glycerol solution to stop the reaction. Approximately 10 muscle fibers per muscle were randomly selected, and drawn using a camera lucida mounted on a Leica binocular scope. Drawings including a scale bar were scanned and muscle fiber lengths were measured using Image J 1.52 (National Institutes of Health, USA). The physiological cross-sectional area (PCSA) of each muscle was calculated by dividing muscle volume by the mean fiber length. We identified 12 jaw muscle bundles representing five functional groups. The jaw openers included *m. depressor mandibulae* (mDM). The group of the external adductors included the *m. adductor mandibulae externus pars superficialis anterior* (mAMESA) and *posterior* (mAMESP), the *pars medialis* (mAMEM), and the *profundus* (mAMEP). The *m. adductor mandibulae posterior* (mAMP) was considered part of this group although it is not an external adductor *sensu stricto*. The group of the pseudotemporalis muscles was composed of *m. pseudotemporalis superficialis* (mPSTS) and *profundus* (mPSTP). The pterygoids included *m. pterygoideus pars lateralis* (mPTL) and

Table 1. Definitions of the anatomical landmarks (LM).

Skull	LM n°	Mandible
Anterior tip of the premaxillar	1	Anterior tip of the dentary
Most medial anterior part of nasal opening	2	Antero-lateral tip of the coronoid
Dorsal point of nasal at the midline	3	Antero-lateral junction between the angular and the surangular
Lateral dorsal protuberance of nasal	4	Antero-lateral tip of the surangular
Anterior end of the joint between the internasal scales	5	Junction between the dentary, the coronoid and the surangular
Anterior corner of the frontal scale	6	Posterior border of the angular foramen below the coronoid
Antero-lateral corner of the frontal scale	7	Dorso-lateral edge of the coronoid
Postero-lateral corner of the frontal scale	8	Dorsal tip of the coronoid
Posterior corner of the frontal scale	9	Dorsal posterior most constriction of the coronoid
Lateral corner of the fronto-parietal scale	10	Mid distance between landmarks 9 and 11
Anterior corner of the interparietal scale	11	Posterior junction between the coronoid and the surangular
Antero-lateral corner of the interparietal scale	12	Junction between the surangular, the angular and the articular
Postero-lateral corner of the interparietal scale	13	Posterior tip of the retroarticular process
Most posterior part of the junction between parietal and occipital scales	14	Antero-ventral junction between the angular and the articular
Junction between the lacrymal, the maxillar and the prefrontal bones	15	Antero-lateral corner of the articular surface
Ventro-medial tip of the frontal bone	16	Postero-lateral corner of the articular surface
Anterior tip of jugal	17	Medial edge of the retroarticular process
Posterior tip of the maxillar, at the junction with the jugal	18	Maximum of curvature between the points 17 and 19
Antero-lateral tip of the pterygoid, at the junction with the ectopterygoid	19	Postero-medial corner of the articular surface
Posterior tip of the jugal	20	Antero-medial corner of the articular surface
Dorsal tip of the jugal	21	Posterior edge of the adductor fossa
Anterior tip of the squamosal	22	Anterior edge of the adductor fossa
Anterior part of the junction between the epipterygoid and the pterygoid	23	Hollow between the posterior and the medial ridges of the coronoid
Dorsal tip of the epipterygoid	24	Postero-ventral tip of the medial ridge of the coronoid
Maximum of curvature of the alar process of prootic	25	Dorsal tip of the medial ridge of the coronoid
Maximum of curvature of the anterior semi-circular canal	26	Dorso-medial tip of the coronoid
Anterior tip of the alar process of sphenoid	27	Antero-ventral tip of the medial ridge of the coronoid
Dorsal tip of the alar process of sphenoid	28	Maximum of curvature of the ventro-medial hollow of the coronoid
Lateral maximum of curvature of the crista prootica	29	Junction between the prearticular, the angular and the splenial
Medial tip of the jugal, at the junction with the ectopterygoid	30	Antero-medial tip of the coronoid
Ventral tip of the postorbital	31	Posterior edge of the Meckelian foramen
Posterior tip of the pterygoid	32	Anterior edge of the Meckelian foramen
Posterior tip of the squamosal	33	Dorso-anterior tip of the dentary
Posterior tip of the paroccipital process of the parietal	34	
Posterior most point of the parietal at the midline	35	
Maximum of curvature of the posterior ridge of the occipital	36	
Ventral bead surrounding the fenestra ovalis	37	
Junction between the vomer and the premaxillar	38	
Anterior junction between the palatin and the maxillar	39	

(Continued)

Table 1. (Continued).

Skull	LM n°	Mandible
Posterior junction between the palatin and the maxillar	40	
Anterior tip of the ectopterygoid, at the junction with the maxillar	41	
Posterior tip of the palatin, at the junction with the pterygoid	42	
Postero-medial tip of the ectopterygoid, at the junction with the pterygoid	43	
Anterior tip of the basipterygoid process	44	
Posterior tip of the basipterygoid process	45	
Lateral process of the basioccipital	46	
Lateral process of the basioccipital	47	
Top of the medial parasagittal bead of the quadrate	48	
Antero-ventro-medial tip of the quadrate	49	
Antero-ventro-medial tip of the quadrate	50	
Maximum of curvature of the anterior face of the quadrate	51	
Postero-ventro-lateral tip of the quadrate	52	
Postero-ventro-medial tip of the quadrate	53	
Postero-dorsal tip of the quadrate, at the junction with the supratemporal	54	

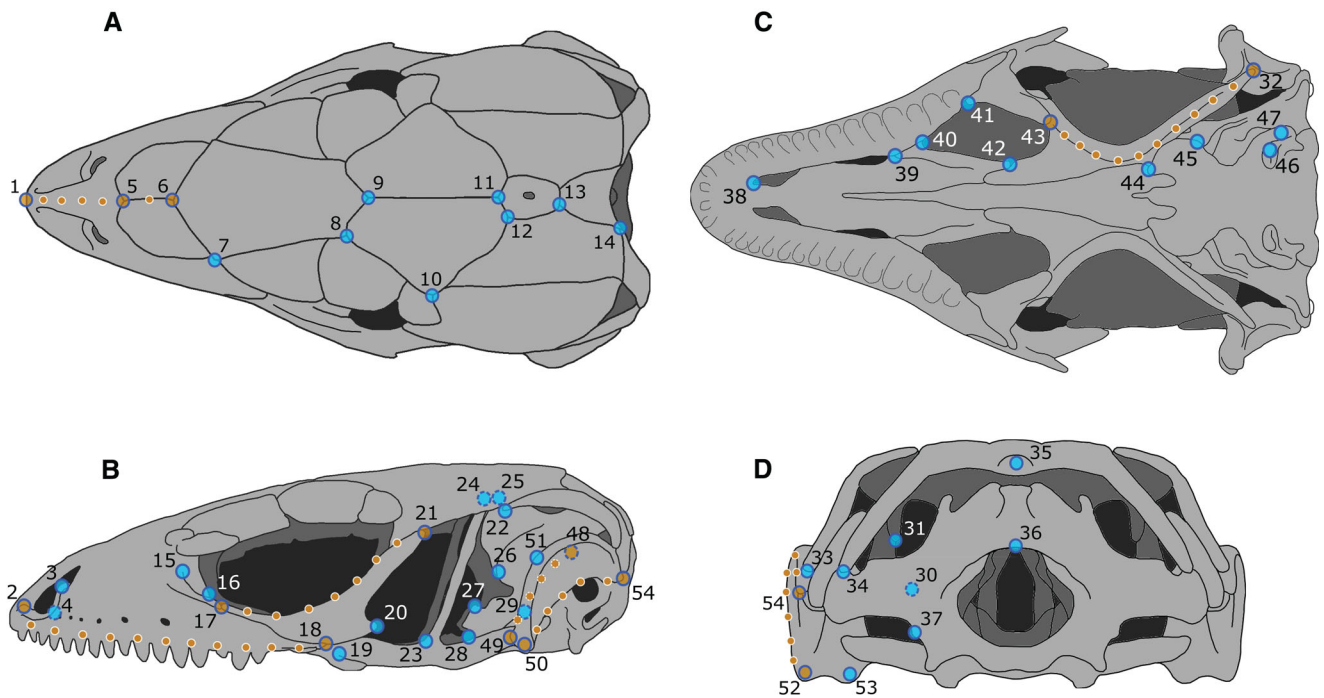


Figure 1. Illustration of the landmarks used to quantify the shape of the cranium. Large blue circles represent anatomical landmarks and small orange circles represent sliding landmarks on curves (a-b-c-d: dorsal, left lateral, ventral, caudal views of the skull).

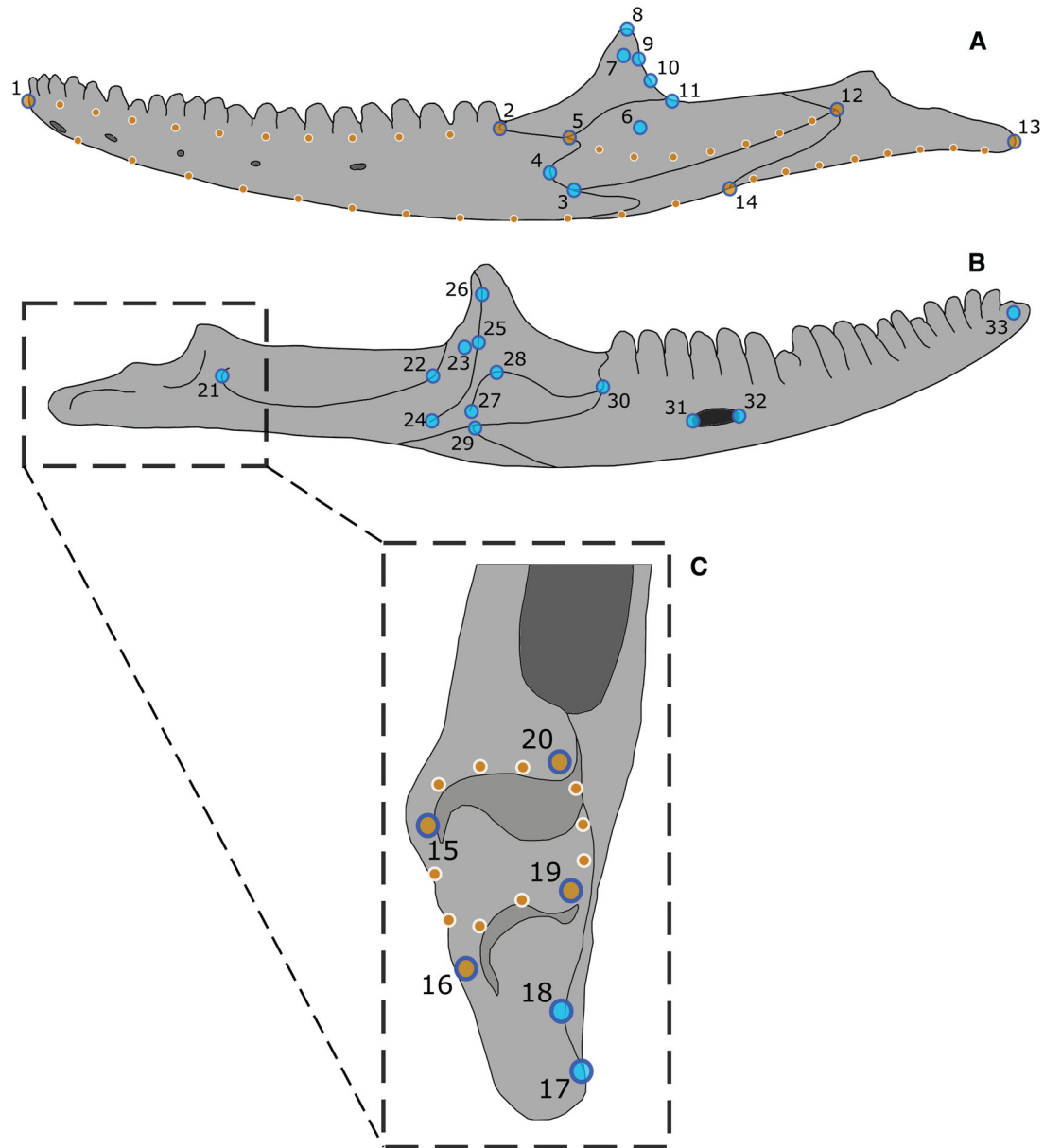


Figure 2. Illustration of the landmarks used to quantify the shape of the mandible. Large blue circles represent anatomical landmarks and small orange circles represent sliding landmarks on curves (a-b-c: left lateral and medial views of the left mandible, and dorsal focus on the retro-articular process).

medialis (mPTM), while the constrictor dorsalis muscles encompassed the *m. levator pterygoidei* (mLPT) and *m. protractor pterygoidei* (mPPT).

STATISTICAL ANALYSES

All statistical analyses were performed using R (R Core Team 2020). Bite force and muscle data were \log_{10} -transformed, proportions of the type of food consumed (e.g., plants, hard arthropods) were arcsine-transformed, and the homogeneity of variances and normality of the distribution of the residuals were verified using Bartlett and Shapiro tests, respectively. For anal-

yses including phylogeny we used a previously published tree describing the relationships between the populations in this study system (see Taverné et al. 2020). Preliminary genomic analyses (Sabolić et al. in preparation) indicated that there is effectively no gene flow between populations, and thus treating them as independent evolving lineages for phylogenetic comparative analyses is justified. Mentions of residual data in all subsequent analyses refer to the residuals of the variables extracted from simple or multivariate regressions on size (more specifically, the centroid size of the skull) performed on the sub-dataset considered (e.g., all females, or females of a single species).

The effect of sex and species on the muscle architecture variables (including the summed muscle mass, the average fiber length, and the summed PCSA of each muscle group) was investigated by means of a two-way multivariate analysis of covariance (MANCOVA, “mancova” function, “jmv” package) with the centroid size of the skull (Csize) as co-variable. MANCOVAs with Csize as co-variable were subsequently performed to test for differences between sexes and localities within each species. Permutation tests were performed (1000 iterations, with randomization of the residuals) to examine the effect of Csize (of the skull or the mandible, depending on the situation), sex, and species, and the effect of Csize, sex, and locality on the mandible and skull shape, using the function “procD.lm” function (“geomorph” package, Adams & Otárola-Castillo, 2013).

Next, muscle and morphological data were averaged by population and by sex. Relationships between all muscle variables (mass, fiber length, and PCSA), bite force, the proportion of plants consumed, the proportion of hard prey consumed, and sexual dimorphism in head dimensions were investigated in males and females separately given the known sexual dimorphism in these species. To do so, stepwise regressions were performed either on raw or on residual muscular data (generated by regressing traits against skull Csize) using the function “stepAIC,” or using the function “phylostep” (“phylolm” package) when accounting for phylogeny.

The contribution of allometry to the observed variability in shape was estimated using a Procrustes ANOVA with permutation (“procD.lm” function) that tested the relationship between the Procrustes coordinates and the centroid size of either the skull or the mandible of each specimen (the “procD.pgls” function was used when including phylogeny).

The relationships between mandible or skull shape and muscle variables, muscle residual variables (obtained after multiple regressions on skull Csize or mandible Csize), bite force, residual bite force, and ecological variables were assessed by running two-block partial least-squares (2b-PLS) regressions using the function “two.b.pls” (“geomorph” package), or using the function “phylo.integration” (“geomorph” package) when accounting for phylogeny. The contributions of the variables included in the tested block to the covariation axis were extracted. Then, these interspecific patterns of covariation between morphology, musculature, performance, and ecology were compared with those occurring at the intraspecific level. To do so, additional 2b-PLS regressions were computed for each sex in each species. The coefficient of correlation between scores of projected values on the first singular vectors of the two blocks (rPLS), accounting for the strength of the covariation axis, was extracted for each 2b-PLS regression. The rPLS of 2b-PLS regressions performed at different levels (intra or interspecific) were compared using the function “compare.pls” (“geomorph” package).

Finally, additional two-block partial least-squares regressions were used to investigate the relationships between the residual muscular variables (again, obtained by a regression on mandible or skull Csize), diet variables, and the allometry-free (AF) mandible and skull shape (obtained with the functions “CAC” and “showPC” - “morpho” package). The covariation patterns at the inter and intraspecific levels were compared as detailed previously. All shape changes associated with the covariation patterns were extracted using the function “tps3d” (“morpho” package).

Results

INTER-POPULATION VARIABILITY IN MUSCLE ARCHITECTURE AND SHAPE

The results of the two-way MANCOVAs carried out on the muscle architecture variables are summarized in Table 2 and show that muscle architecture differs between sexes and species. The effect of Csize was also significant. A significant interaction between sex and species was also detected prompting us to run analyses for each species separately. A subsequent MANCOVA found significant sex, locality, and Csize effects for *P. melisellensis*. No interaction between sex and locality was detected. The same patterns were detected for *P. sicula* (Table 2).

The results of the permutation analyses carried out on cranial and mandible shape are summarized in Table 3, and variability in morphology within the dataset is illustrated in Supporting Information 1. The tests performed on the mandible shapes of all specimens revealed significant effects of Csize, sex, species, and the interaction between Csize and species. In *P. melisellensis*, significant effects of Csize, sex, locality, and the interaction between Csize and locality were detected. In *P. sicula*, significant effects of Csize, sex, and locality were detected, as well as interaction effects between Csize and sex, and between sex and locality. The permutation tests, performed on the skull shape of all specimens showed an effect of Csize, sex, species, as well as the interaction between Csize and species, and between sex and species. In *P. melisellensis*, the tests revealed an effect of Csize, sex and locality, and the interaction between sex and locality. In *P. sicula*, the tests revealed an effect of Csize, sex, and locality, and the interaction between Csize and sex.

RELATIONSHIPS BETWEEN MUSCLE ARCHITECTURE, BITE FORCE, AND ECOLOGY

The physiological cross-sectional area (PCSA) of the jaw muscles explained variation in bite force (Table 4). In females, greater absolute ($R^2 = 0.85$, $P < 0.001$) and residual ($R^2 = 0.71$, $P = 0.001$) bite force was associated with relatively stronger external adductors and weaker pseudotemporalis muscles. In males, an

Table 2. Results of the analyses of covariance carried out on muscle architecture data at the individual level, either on the whole dataset or for each species separately (df: degrees of freedom, P: P-value).

		Wilk's λ	F	df	P
Entire data set	Species	0.490	8.77	1	0.001
	Sex	0.280	21.85	1	0.001
	Csize	0.340	16.50	138	0.001
	Species x Sex	0.780	2.38	1	0.006
		Wilk's λ	F	df1	P
<i>P. melisellensis</i>	Locality	0.005	3.17	9	0.001
	Sex	0.110	29.10	1	0.001
	Csize	0.640	2.01	79	0.036
	Locality x Sex	0.220	1.30	5	0.080
		Wilk's λ	F	df1	P
<i>P. sicula</i>	Locality	0.013	2.76	5	0.001
	Sex	0.240	7.33	1	0.001
	Csize	0.350	4.24	58	0.001
	Locality x Sex	0.190	0.96	5	0.610

Bold values are statistically significant.

Table 3. Results of the permutation tests carried out on shape data at the individual level, either on the whole dataset or for each species separately (df: degrees of freedom, R²: coefficient of determination, F: F statistic, Z: effect sizes based on F distribution, P: P-value).

		Skull					Mandible				
		df	R ²	F	Z	P	df	R ²	F	Z	P
Whole dataset	Csize	1	0.213	41.78	7.66	0.001	1	0.265	56.92	8.11	0.001
	species	1	0.059	11.73	5.55	0.001	1	0.067	14.47	6.85	0.001
	sex	1	0.016	3.06	2.60	0.010	1	0.027	5.79	4.84	0.001
	Csize:species	1	0.012	2.36	2.09	0.031	1	0.013	2.74	2.89	0.004
	Csize:sex	1	0.007	1.42	0.97	0.177	1	0.006	1.21	0.71	0.232
	species:sex	1	0.012	2.44	2.27	0.019	1	0.007	1.56	1.36	0.088
	Csize:species:sex	1	0.011	2.08	1.75	0.058	1	0.005	0.98	0.10	0.454
<i>P. melisellensis</i>	Csize	1	0.272	40.79	6.78	0.001	1	0.347	62.47	7.37	0.001
	sex	1	0.028	4.23	3.43	0.001	1	0.022	4.03	3.58	0.001
	locality	9	0.211	3.51	6.53	0.001	9	0.231	4.63	9.49	0.001
	Csize:sex	1	0.013	1.99	1.64	0.071	1	0.009	1.55	1.39	0.086
	Csize:locality	9	0.066	1.10	0.53	0.285	9	0.072	1.45	2.59	0.005
	sex:locality	5	0.058	1.76	2.22	0.018	5	0.027	0.99	0.06	0.463
	Csize:sex:locality	5	0.032	0.98	-0.01	0.478	5	0.025	0.91	-0.49	0.691
<i>P. sicula</i>	Csize	1	0.121	11.52	5.08	0.001	1	0.196	19.92	6.93	0.001
	sex	1	0.046	4.38	3.25	0.002	1	0.067	6.80	4.95	0.001
	locality	5	0.269	5.15	6.37	0.001	5	0.192	3.90	7.19	0.001
	Csize:sex	1	0.023	2.22	1.94	0.043	1	0.022	2.24	2.47	0.007
	Csize:locality	5	0.061	1.17	0.77	0.225	5	0.049	1.01	0.09	0.461
	sex:locality	5	0.052	1.00	0.02	0.470	5	0.076	1.53	2.41	0.007
	Csize:sex:locality	5	0.061	1.18	0.68	0.249	5	0.052	1.06	0.37	0.368

Bold values are statistically significant (< 0.05).

Table 4. Results of the multiple regressions between bite force (BF), the proportion of plants (PLANT), the proportion of hard prey items (HARD), the sexual dimorphism in head dimensions (SDhead) and the PCSA of the 5 muscle groups (DM: jaw opener, ADD: external adductors, PSEU: pseudotemporalis, PTG: pterygoids, CONST: constrictor dorsalis muscles).

		Females		Males		
		Raw	Residuals	Raw	Residuals	
No correction for phylogeny	Model	$P < 0.001$	$P = 0.001$	$P = 0.04$	$P = 0.084$	
		$R^2 = 0.854$	$R^2 = 0.71$	$R^2 = 0.3$	$R^2 = 0.212$	
	DM					
	ADD	$s = 2.838$	$\beta = 0.35$	$s = 3.06$	$\beta = 0.16$	
	PSEU	$s = -1.384$	$\beta = -0.20$	$s = -1.212$	$\beta = -0.07$	
	PTG			$s = -1.231$	$\beta = -0.13$	
	CONST					
	PLANT	Model	$P = 0.012$	$P = 0.013$	$P = 0.013$	$P = 0.037$
			$R^2 = 0.541$	$R^2 = 0.422$	$R^2 = 0.53$	$R^2 = 0.423$
	HARD	Model	$P = 0.033$	$P = 0.030$	$P = 0.113$	$P = 0.008$
		$R^2 = 0.425$	$R^2 = 0.439$	$R^2 = 0.175$	$R^2 = 0.574$	
With correction for phylogeny	DM					
	ADD	$s = -4.607$	$\beta = -0.56$	$s = -4.455$	$\beta = -0.23$	
	PSEU				$s = -3.955$	
	PTG	$s = 4.167$	$\beta = 0.53$	$s = 3.592$	$\beta = 0.15$	
	CONST				$s = 2.729$	
	SDhead	Model	$P = 0.004$	$P = 0.198$	$P = 0.040$	$P = 0.150$
			$R^2 = 0.540$	$R^2 = 0.077$	$R^2 = 0.289$	$R^2 = 0.138$
				$s = 0.991$	$\beta = 0.09$	$s = -0.703$
						$\beta = -0.05$
				$s = -1.311$	$\beta = -0.14$	
	Model	$\sigma^2 < 0.001$	$\sigma^2 = 0.001$	$\sigma^2 = 0.001$	$\sigma^2 = 0.001$	
DM						
ADD	$s = 3.451$	$P = 0.003$	$s = 3.493$	$P = 0.003$	$s = 2.568$	
					$P = 0.013$	
					$s = 3.193$	
					$P = 0.007$	

(Continued)

Table 4. (Continued).

	Females		Males	
	Raw	Residuals	Raw	Residuals
PSEU	$s = -2.065$	$P = 0.023$	$s = -2.097$	$P = 0.024$
PTG			$s = -1.934$	$P = 0.029$
CONST				$s = -2.009$
				$P = 0.020$
PLANT				
Model	$\sigma^2 = \mathbf{0.011}$	$\sigma^2 = 0.021$	$\sigma^2 = \mathbf{0.008}$	$\sigma^2 = \mathbf{0.009}$
DM			$s = 1.768$	$s = 1.395$
			$s = 7.384$	$s = 5.595$
ADD				$P = 0.049$
PSEU	$s = 5.709$	$P = 0.043$		
PTG	$s = -3.333$	$P = 0.156$	$s = -5.523$	$P = 0.027$
CONST			$s = -2.771$	$P = 0.011$
				$s = -4.222$
HARD				$P = 0.101$
Model	$\sigma^2 = \mathbf{0.003}$	$\sigma^2 = \mathbf{0.003}$	$\sigma^2 = \mathbf{0.008}$	$\sigma^2 = \mathbf{0.002}$
DM	$s = -1.891$	$P = 0.025$	$s = -1.852$	$P = 0.037$
	$s = -2.840$	$P = 0.139$	$s = -2.752$	$P = 0.104$
ADD			$s = -2.506$	$P = 0.092$
PSEU			$s = 3.245$	$P = 0.039$
PTG	$s = 3.920$	$P = 0.040$		$s = 4.345$
CONST				$s = 2.599$
				$P = 0.004$
SDhead				
Model	$\sigma^2 = \mathbf{0.003}$	$\sigma^2 = \mathbf{0.002}$	$\sigma^2 = \mathbf{0.001}$	$\sigma^2 = \mathbf{0.002}$
DM				
ADD	$s = -2.104$	$P = 0.129$	$s = -1.736$	$P = 0.098$
			$s = -1.985$	$P = 0.079$
PSEU			$s = 1.361$	$P = 0.094$
PTG			$s = 0.977$	$P = 0.083$
CONST				$s = 1.049$
				$P = 0.222$

s: slope, β : standardized coefficient, R^2 : coefficient of determination, P: p-value. Bold values indicate retained models. Values in blue and red indicate a negative and a positive correlation, respectively.

increase in absolute bite force ($R^2 = 0.30$, $P = 0.04$) was associated with stronger external adductors and weaker pterygoid muscles. These results held when accounting for phylogeny.

The proportion of plants consumed was also significantly correlated with the absolute and relative PCSA of jaw adductor muscles in both females and males (absolute data in females: $R^2 = 0.54$, $P = 0.012$; in males: $R^2 = 0.53$, $P = 0.013$; residual data in females: $R^2 = 0.42$, $P = 0.013$; in males $R^2 = 0.42$, $P = 0.037$). In females, a higher proportion of plants in the diet was associated with relatively stronger pseudotemporalis muscles and weaker pterygoids. In males, an increase in the amount of plant material in the diet was associated with relatively stronger jaw openers and external adductors, and relatively weaker pterygoids and constrictor dorsalis muscles. These results were largely upheld when accounting for phylogeny (Table 4).

The multiple regressions also revealed a significant association between the proportion of hard prey items consumed and the PCSA of the jaw muscles in females ($R^2 = 0.43$, $P = 0.033$) and residual PCSA in both females and males (females: $R^2 = 0.44$, $P = 0.030$; males: $R^2 = 0.57$, $P = 0.008$). In females, a greater proportion of hard prey was associated with stronger pterygoids and relatively weaker external adductors. In males, the same pattern was observed but the PCSA of the pseudotemporalis muscles was also associated with an increase in hard prey in the diet. Despite some small differences, the results of these regressions remained consistent when accounting for phylogeny (Table 4).

The sexual dimorphism in head dimensions, which was considered here as a proxy for the intensity of sexual competition, correlated with the absolute PCSA of the jaw muscles in both females ($R^2 = 0.54$, $P = 0.004$) and males ($R^2 = 0.29$, $P = 0.040$). In females, a higher dimorphism was associated with weaker pterygoid muscles, whereas it was associated with weaker pseudotemporalis muscles and stronger jaw openers in males. When accounting for phylogeny, a higher dimorphism correlated with relatively stronger pseudotemporalis muscles in both females and males, and with relatively stronger pterygoids in males (Table 4).

ALLOMETRY

Allometry explained a significant part of the variability in skull and mandible shape in males and females at the intra and interspecific levels (Table 5). For example, allometry explained 13.4% and 18.0% of the total variation in mandible and cranium shape, respectively (all $P = 0.001$). In males, allometry explained 9.7% and 7.1% of the total variation in mandible and cranial shape (all $P = 0.001$). When accounting for phylogeny, allometries were no longer significant ($P > 0.05$). Although they were significant,

allometry trajectories did not differ much between species (Supporting Information 2).

CO-VARIATION BETWEEN HEAD SHAPE, PERFORMANCE, MUSCLE ARCHITECTURE, AND ECOLOGY

For both sexes of each species, the 2b-PLS analyses at the interspecific level revealed that mandible and cranial shapes significantly covaried with bite force (except in males), muscular, and ecological variables (Table 6). Most patterns of covariation still held when accounting for the phylogeny. Residual musculature variables and ecology also strongly covaried with cranial and mandible shape corrected for allometry, in both females and males, even when correcting for phylogeny (except in a few cases, see Table 6). The PCSA and the volume of three muscle groups, the external adductors, the pseudotemporalis muscles, and the pterygoids were the muscular variables that drove this covariation (Supporting Information 3). On the other hand, the proportion of plants consumed was the ecological variable that best explained the covariation between ecology and cranial shape. In all cases, the shapes associated with bigger and stronger muscles were similar to those associated with a higher proportion of plants consumed. Specifically, an increase in muscle PCSA as well as an increased consumption of plants were both associated with an increased overall robustness of the mandible, with larger areas for muscle insertions (e.g., the coronoid process as the insertion site for pseudotemporalis muscles, or the lateral side of the mandible serving as an attachment site for external adductors). Additionally, the snout was pointier, the skull was taller (mostly due to a more pronounced ventral curvature of the pterygoid bone), and presented a wider temporal window and a more curved quadrate (Fig. 3).

No pattern of covariation was detected between residual bite force and shape or residual bite force and allometry-free shape, whereas a few significant patterns were detected between residual musculature and cranial or mandible shape (Table 6). For instance, the skull shape of males covaried with residual jaw musculature (especially the PCSA and the volume of the external adductors, the pseudotemporalis muscles, and the pterygoids, see Supporting Information 3). The skull shape variation was somewhat similar to that described above, except that the increase in skull height was enabled by a rounder skull roof instead of having a more ventrally curved pterygoid bone. Residual musculature variables and ecological variables also covaried with allometry-free skull and mandible shape (Table 6), yet covariation patterns differed by sex. In females, stronger and larger constrictor dorsalis muscles were associated with a narrower posterior section of the skull, characterized by quadrates and posterior processes of the parietals pushed toward the midsagittal plane. In males, relatively stronger and bigger external adductors,

Table 5. Results of the Procrustes ANOVAs with permutation testing for the effect of allometry on observed variation in mandible and skull shape.

	Without correction for phylogeny				With correction for phylogeny			
	Skull		Mandible		Skull		Mandible	
Females	P = 0.001 *	F = 8.965	P = 0.001 *	F = 12.732	P = 0.453	F = 0.879	P = 0.030 *	F = 2.728
	R ² = 0.134	Z = 4.362	R ² = 0.180	Z = 6.058	R ² = 0.081	Z = 0.076	R ² = 0.214	Z = 1.793
Males	P = 0.001 *	F = 8.237	P = 0.001 *	F = 5.919	P = 0.415	F = 0.952	P = 0.281	F = 1.209
	R ² = 0.097	Z = 4.796	R ² = 0.071	Z = 4.671	R ² = 0.064	Z = 0.154	R ² = 0.079	Z = 0.643
<i>P. melisellensis</i>	P = 0.001 *	F = 29.085	P = 0.001 *	F = 40.809	P = 0.291	F = 1.118	P = 0.178	F = 1.492
	R ² = 0.272	Z = 6.229	R ² = 0.343	Z = 6.678	R ² = 0.121	Z = 0.238	R ² = 0.094	Z = 0.847
<i>P. sicula</i>	P = 0.001 *	F = 7.810	P = 0.001 *	F = 13.805	P = 0.624	F = 0.636	P = 0.744	F = 0.524
	R ² = 0.121	Z = 4.380	R ² = 0.195	Z = 6.159	R ² = 0.089	Z = -0.162	R ² = 0.071	Z = -0.289
Females <i>P. melisellensis</i>	P = 0.004 *	F = 4.648	P = 0.017 *	F = 2.327	P = 0.846	F = 0.448	P = 0.625	F = 0.719
	R ² = 0.142	Z = 3.153	R ² = 0.077	Z = 2.195	R ² = 0.101	Z = -0.922	R ² = 0.152	Z = -0.293
Males <i>P. melisellensis</i>	P = 0.001 *	F = 5.809	P = 0.001 *	F = 4.663	P = 0.213	F = 1.413	P = 0.604	F = 0.729
	R ² = 0.108	Z = 4.088	R ² = 0.089	Z = 3.783	R ² = 0.150	Z = 0.808	R ² = 0.083	Z = -0.273
Females <i>P. sicula</i>	P = 0.199	F = 1.419	P = 0.001 *	F = 2.901	P = 0.588	F = 0.575	P = 0.098	F = 3.009
	R ² = 0.048	Z = 0.838	R ² = 0.094	Z = 2.916	R ² = 0.126	Z = -0.396	R ² = 0.429	Z = 1.565
Males <i>P. sicula</i>	P = 0.040 *	F = 2.292	P = 0.001 *	F = 4.731	P = 0.911	F = 0.385	P = 0.186	F = 1.377
	R ² = 0.078	Z = 1.916	R ² = 0.149	Z = 4.286	R ² = 0.088	Z = -1.218	R ² = 0.256	Z = 0.623

Bold values indicate statistically significant influence of allometry ($P < 0.05$).

P, P-value; F, F-statistic; R², coefficient of determination; Z, effect sizes based on F distribution.

pseudotemporalis muscles, and pterygoids were associated with a more robust mandible, a bigger coronoid process, and taller skull roof, a more ventrally curved pterygoid bone, and a shorter snout. In males, similar deformations were observed associated with an increase in the proportion of hard items in the diet (Fig. 4). Similar patterns were generally detected when accounting for the phylogeny (Table 6).

COMPARISON OF THE EVOLUTIONARY TRAJECTORIES

The rPLS of each 2b-PLS were compared to explore whether the strength of the patterns of covariation was similar between sexes, species, and at the intra- (Supporting Information 4) and inter-specific levels (Table 6, 7). Overall, we found no or little statistical difference in the strength of the covariation. The nature of the covariations between ecology, muscles architecture, and morphology also appeared qualitatively similar, as illustrated by the comparison in covariation pattern between muscle architecture and skull shape in males of *P. melisellensis* and in all males, for example (Fig. 5). Indeed, the increase in the same set of mus-

cle architecture variables (the mass and PCSA of the adductor muscle groups) contributes to similar morphological variation (a wider temporal window, enabled by a higher skull roof, a pterygoid bone that is more ventrally and medially curved, a more curved quadrate, a more vertical jugal).

Discussion

DIFFERENCES IN SELECTIVE REGIMES ACROSS INDEPENDENT INSULAR POPULATIONS

The populations included in the present study vary greatly in their ecology as they inhabit islands that differ in their size and habitat structure (Taverne et al. 2019). Island area and island isolation further influence the diversity and the abundance of resources available, predation pressure, and population densities that together drive ecological dynamics (Novosolov & Meiri, 2013; Novosolov et al. 2016, Whittaker et al. 2017; Itescu et al. 2019). In the Adriatic archipelago, the lizard populations present dietary specializations, ranging from a strictly insectivorous diet to an omnivorous diet including a majority of plant items (Taverne

Table 6. Results of the two-block partial least-squares analyses (2b-PLS) between bite force (BF), muscular data (muscle PCSA, mass and fiber length), ecology (proportion of plants and hard items consumed, and the level of intraspecific competition) and 3D morphology at the population level.

		Without correction for phylogeny				With correction for phylogeny				
		Female		Male		Female		Male		
		Skull	Mandible	Skull	Mandible	Skull	Mandible	Skull	Mandible	
BF	<i>P</i>	0.005	0.001	0.131	0.351	0.036	0.445	0.398	0.465	Raw shape
	rPLS	0.831	0.866	0.637	0.655	0.756	0.616	0.598	0.590	
	%covar	100	100	100	100	-	-	-	-	
Musculature	<i>P</i>	0.003	0.002	0.011	0.067	0.001	0.045	0.042	0.080	
	rPLS	0.855	0.905	0.782	0.727	0.946	0.827	0.771	0.739	
	%covar	96.560	96.878	87.127	88.219	-	-	-	-	
Ecology	<i>P</i>	0.017	0.013	0.019	0.011	0.281	0.422	0.037	0.014	
	rPLS	0.790	0.815	0.769	0.868	0.661	0.664	0.782	0.831	
	%covar	90.397	90.310	68.359	74.995	-	-	-	-	
rBF	<i>P</i>	0.622	0.768	0.306	0.291	0.089	0.378	0.320	0.506	
	rPLS	0.538	0.599	0.626	0.649	0.723	0.644	0.623	0.579	
	%covar	100	100	100	100	-	-	-	-	
rMusculature	<i>P</i>	0.393	0.764	0.036	0.195	0.001	0.061	0.008	0.063	
	rPLS	0.708	0.771	0.874	0.833	0.941	0.844	0.841	0.787	
	%covar	63.232	53.887	61.496	60.359	-	-	-	-	
rBF	<i>P</i>	0.411	0.414	0.180	0.145	0.399	0.446	0.184	0.293	AF shape
	rPLS	0.749	0.689	0.748	0.649	0.629	0.623	0.679	0.705	
	%covar	100	100	100	100	-	-	-	-	
rMusculature	<i>P</i>	0.005	0.119	0.001	0.043	0.001	0.027	0.006	0.048	
	rPLS	0.904	0.859	0.877	0.844	0.963	0.883	0.858	0.827	
	%covar	63.013	54.795	66.935	65.803	-	-	-	-	
Ecology	<i>P</i>	0.649	0.213	0.001	0.001	0.192	0.351	0.023	0.011	
	rPLS	0.898	0.793	0.892	0.845	0.729	0.681	0.810	0.875	
	%covar	61.512	86.521	42.825	76.967	-	-	-	-	

Also listed are the results of analyses using residual data (r) against raw shapes and allometry-free shapes (AF). *P*: *P*-value, rPLS: coefficient of covariation, % covar: percentage of covariance explained by the PLS axis considered. Bold values are statistically significant ($P < 0.05$) and associated results are highlighted in grey.

et al. 2019). The consumption of mechanically resistant items (e.g., hard arthropods, plant material) was observed on the smallest and the most depauperate islands. These populations also vary in the intensity of sexual competition, as expressed by the level of sexual dimorphism in head dimensions. Ecological pressures such as sexual competition and the consumption of difficult-to-reduce items are reflected in variation in bite force (Taverne et al. 2020). Additionally, these factors impact muscular anatomy and cranial shape. These patterns differed depending on the trait considered (Tables 4 and 6, Figs. 3 and 4), suggesting that different selective regimes operate on these islands. Because different associations between form and function were detected in males and females, sexes appear to be confronted with different selec-

tive pressures. Interestingly sex-related specificities were replicated among populations within a species, but were species-specific.

EVOLUTION OF PHENOTYPES

The present study allowed us to partly tease apart the drivers of phenotypic variation. Lizards grow continuously during their life (Haines, 1969). For this reason, size is often a central life-history trait enabling rapid responses to environmental fluctuations (Meiri, 2008; Hall & Warner, 2017), especially in insular habitats (Lomolino, 2005; Losos and Ricklefs 2009; Sagonas et al. 2014). A significant part of phenotypic variation often originates from allometric growth in ectotherms like lizards (Urošević

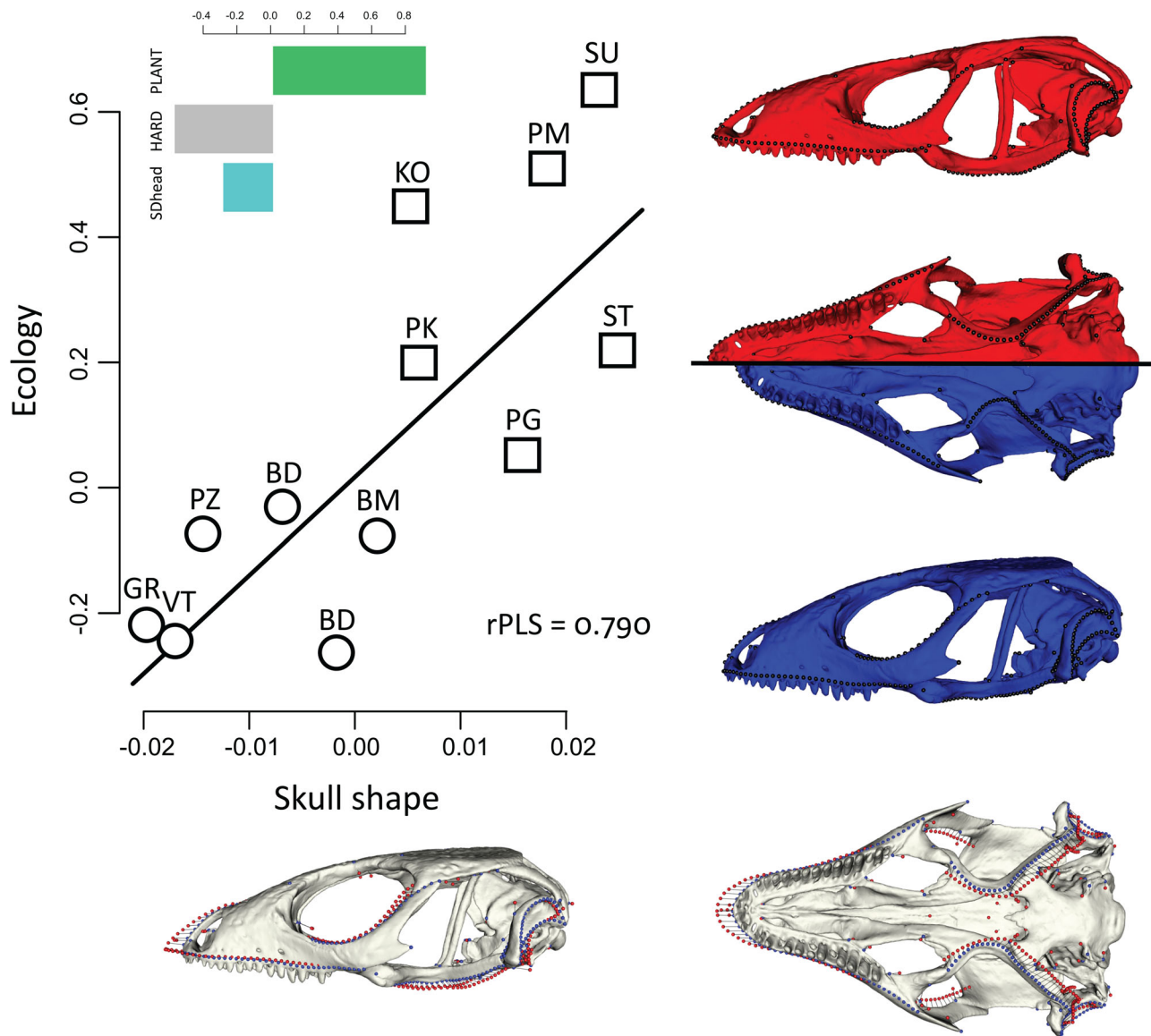


Figure 3. Results of the 2b-PLS analysis exploring the covariation between ecology and skull shape in females (circles: *P. melisellensis* populations, squares: *P. sicula* populations). Red shapes (and red lollipops) represent the theoretical deformations associated with the positive side of the covariation axis (blue shapes: negative side). The histogram gives the contributions of each variable to the axis of covariation. Note the differences in the adductor chamber size, snout length, and the curvature of the quadrate.

et al. 2012a,b). As expected, our results showed that phenotypic variation across populations and sexes was partly explained by allometry (Table 5). Interspecific differences observed here are congruent with diversification along the allometric trajectory (Felsenstein, 1985). Besides allometry, dietary specialization, the intensity of sexual competition, and bite force were important drivers of phenotypic variation.

We found that musculature strongly drives variation in bite force in the two species studied. Moreover, our analyses suggest that this relationship is not purely allometric. An increase in bite force was associated with an increase in the absolute and the relative PCSA of the external jaw adductors in both males and fe-

males (Table 4) suggesting that increasing the force of this muscle group is the most effective way to induce variation in bite force. This is corroborated by previous studies that showed that the external adductor muscles of lizards are the primary drivers of variation in bite force at the interspecific level (Wittorski et al. 2016). In males, the variation in the contribution of the external adductors is largely the result of the variation in muscle volume (Supplementary Information 5). As these muscles are positioned laterally in the head, their volume might be less constrained by other cranial structures than deeper muscle bundles (Rieppel and Gronowski 1981; Herrel et al. 1998; Herrel et al. 2007). Functionally relevant associations between musculature and ecology were

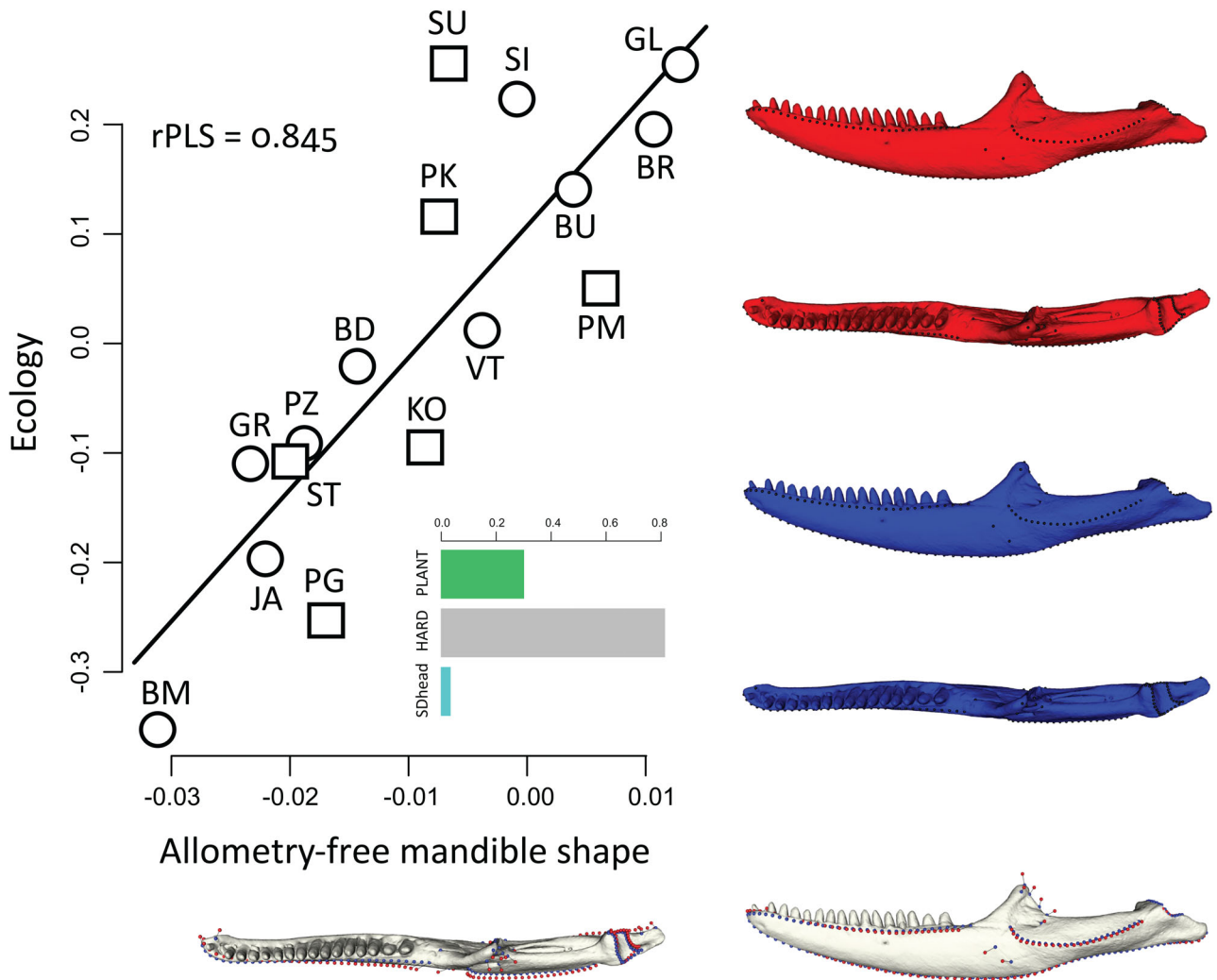


Figure 4. Results of the 2b-PLS analysis exploring the covariation between ecology and allometry-free mandible shape in males (circles: *P. melisellensis* populations, squares: *P. sicula* populations). Red shapes (and red lollipops) represent the theoretical deformations associated with the positive side of the axis of covariation (blue shapes: negative side). The histogram gives the contributions of each variable to the axis of covariation. Note the differences in overall mandible robustness, the thickness of the coronoid process, and the lateral area for muscle insertion.

also detected. The inclusion of greater amounts of plant items in the diet was associated either with stronger pseudotemporalis muscles in females, or with stronger external adductors in males, whereas greater amounts of hard prey in the diet were associated with stronger pterygoids in both sexes. The pterygoids are more efficient at generating bite force at large gape as their moment arm increases significantly with gape (Herrel et al. 1999a, Herrel et al. 1999b). Hence, dietary specialization seems to be allowed by a preferential investment in muscle groups that optimize force generation in a context of biting at low or wide gapes (when eating plant items or hard prey, respectively). The same logic seems to operate in males, with more intense sexual competition, such as male-male combat, going along with more strongly developed pterygoid muscles.

Our analyses of covariation revealed strong associations between ecology, bite force, and muscle architecture on the one hand, and mandible and cranial shape on the other hand. However, the fact that residual bite force and muscle variables only rarely showed significant covariation with shape highlights the influence of size, as corroborated by the significant allometry in the shape of the mandible and cranium in both males and females. The importance of allometric effects in allowing skull shape changes in relation to habitat use is common in lizards (at the intraspecific level: Kaliontzopoulou et al. 2010; at the interspecific level: Urošević et al. 2012a). Yet, residual data showed covariations with allometry-free mandible and cranial shapes, indicating that variation in shape is not explained by allometry alone. Instead, it appears that the covariation between bite

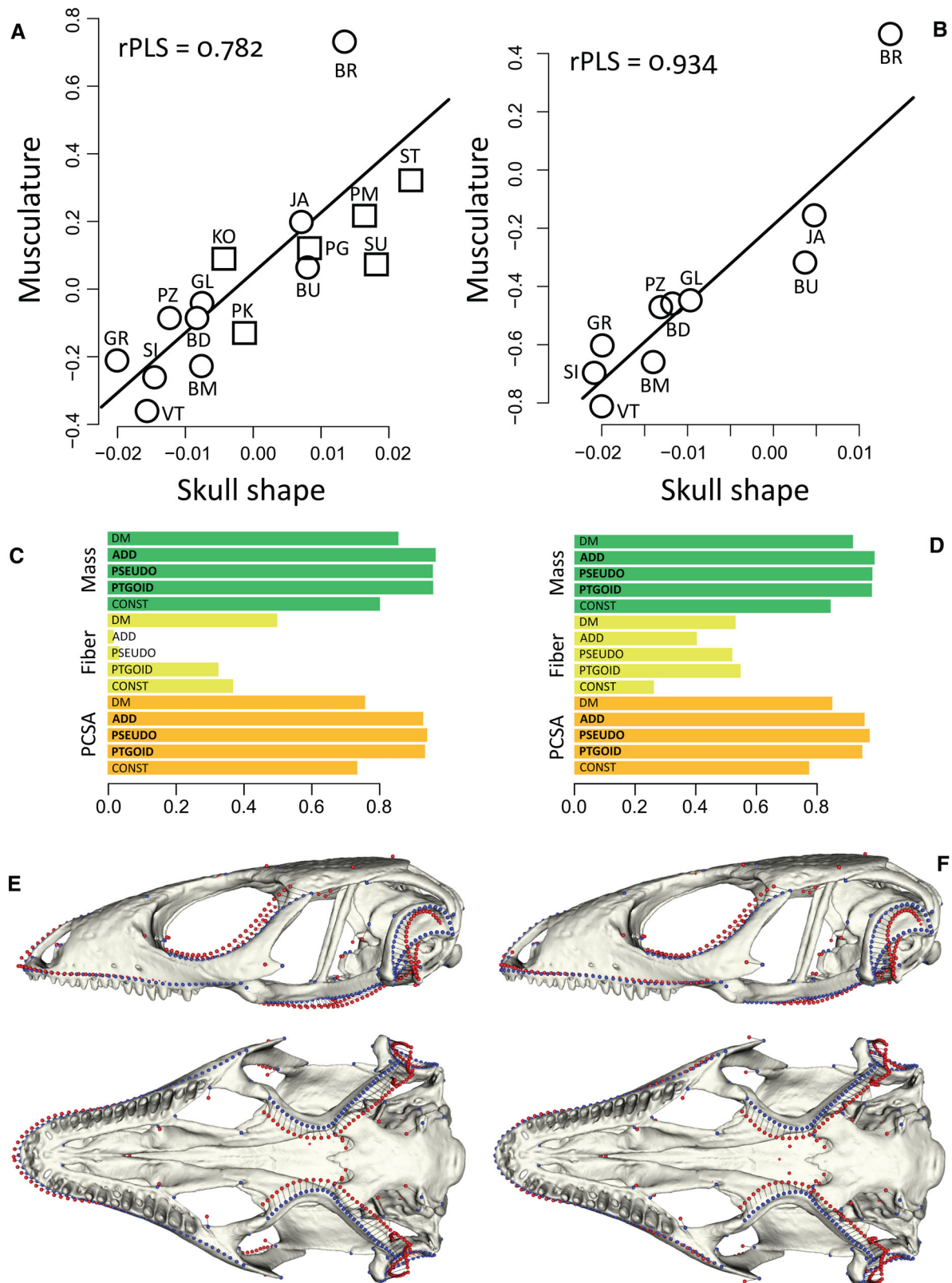


Figure 5. Comparison of the results of the 2b-PLS analysis exploring the covariation between muscle architecture and skull shape in all males (A, C, E) (circles: *P. melisellensis*, squares: *P. sicula*), and in males of *P. melisellensis* populations only (B, D, F). Red lollipops represent the theoretical deformations associated with the positive side of the axis of covariation (blue lollipops: negative side). The histograms give the contributions of each muscular variable to the axis of covariation. Note the differences in the adductor chamber size, snout length, and the curvature of the quadrate and of the pterygoid bone.

Table 7. Comparisons of the covariation patterns at the different levels of biological integration (BF: bite force, res: residual, F: females, M: males, meli: *P. melisellensis*, sicula: *P. sicula*, *P*: *P*-value, rPLS: coefficient of covariation, AF shape: allometry-free shape).

					Skull				Mandible				Raw shape
					<i>P</i>	rPLS 1	rPLS 2	Z-score	<i>P</i>	rPLS 1	rPLS 2	Z-score	
BF	Between sexes	F. meli	x	M. meli	0.219	0.91	0.673	1.227	0.274	0.853	0.617	1.093	
		F. sicula	x	M. sicula	0.832	0.75	0.749	0.212	0.017	0.918	0.605	2.390	
	Between species	F. meli	x	F. sicula	0.504	0.91	0.75	0.668	0.856	0.853	0.918	0.182	
		M. meli	x	M. sicula	0.884	0.673	0.749	0.146	0.549	0.617	0.605	0.598	
	Intra vs. Interspecific	F. meli	x	all females	0.259	0.91	0.831	1.128	0.094	0.853	0.867	1.677	
		F. sicula	x	all females	0.115	0.75	0.831	1.576	0.114	0.918	0.867	1.580	
		M. meli	x	all males	0.522	0.673	0.637	0.641	0.405	0.617	0.655	0.833	
M. sicula		x	all males	0.664	0.749	0.637	0.435	0.088	0.605	0.655	1.709		
Musculature	Between sexes	F. meli	x	M. meli	0.125	0.836	0.934	1.534	0.933	0.828	0.732	0.084	
		F. sicula	x	M. sicula	0.459	0.813	0.946	0.739	0.271	0.978	0.902	1.101	
	Between species	F. meli	x	F. sicula	0.999	0.836	0.813	0.001	0.173	0.828	0.978	1.363	
		M. meli	x	M. sicula	0.456	0.934	0.946	0.746	0.809	0.732	0.902	0.241	
	Intra vs. Interspecific	F. meli	x	all females	0.082	0.836	0.855	1.739	0.024	0.828	0.905	2.263	
		F. sicula	x	all females	0.104	0.813	0.855	1.627	0.176	0.978	0.905	1.353	
		M. meli	x	all males	0.776	0.934	0.782	0.284	0.677	0.732	0.727	0.417	
M. sicula		x	all males	0.662	0.946	0.782	0.437	0.785	0.902	0.727	0.272		
Ecology	Between sexes	F. meli	x	M. meli	0.182	0.869	0.956	1.333	0.007	0.692	0.902	2.702	
		F. sicula	x	M. sicula	0.548	0.837	0.915	0.601	0.966	0.909	0.855	0.041	
	Between species	F. meli	x	F. sicula	0.993	0.869	0.837	0.009	0.046	0.692	0.909	1.994	
		M. meli	x	M. sicula	0.535	0.956	0.915	0.619	0.198	0.902	0.855	1.288	
	Intra vs. Interspecific	F. meli	x	all females	0.335	0.869	0.790	0.964	0.008	0.692	0.815	2.662	
		F. sicula	x	all females	0.355	0.837	0.790	0.925	0.168	0.909	0.815	1.377	
		M. meli	x	all males	0.465	0.956	0.770	0.731	0.984	0.902	0.868	0.024	
M. sicula		x	all males	0.959	0.915	0.770	0.051	0.141	0.855	0.868	1.474		
resBF	Between sexes	F. meli	x	M. meli	0.539	0.822	0.661	0.614	0.479	0.805	0.620	0.706	
		F. sicula	x	M. sicula	0.659	0.728	0.681	0.440	0.044	0.887	0.670	2.005	

(Continued)

Table 7. (Continued).

				Skull				Mandible							
				<i>P</i>	rPLS 1	rPLS 2	Z-score	<i>P</i>	rPLS 1	rPLS 2	Z-score				
	Between species	F. meli	x	F. sicula	0.748	0.822	0.728	0.321	0.509	0.805	0.887	0.659			
		M. meli	x	M. sicula	0.818	0.661	0.681	0.229	0.888	0.620	0.670	0.140			
	Intra vs. Interspecific	F. meli	x	all females	0.687	0.822	0.538	0.402	0.971	0.805	0.599	0.036			
		F. sicula	x	all females	0.917	0.728	0.538	0.105	0.631	0.887	0.599	0.480			
		M. meli	x	all males	0.522	0.661	0.626	0.640	0.439	0.620	0.650	0.774			
		M. sicula	x	all males	0.793	0.681	0.626	0.428	0.281	0.670	0.650	1.079			
resMusculature	Between sexes	F. meli	x	M. meli	0.303	0.869	0.904	1.030	0.311	0.963	0.922	1.013			
		F. sicula	x	M. sicula	0.809	0.915	0.924	0.241	0.503	0.844	0.761	0.669			
	Between species	F. meli	x	F. sicula	0.347	0.869	0.915	0.939	0.172	0.963	0.844	1.367			
		M. meli	x	M. sicula	0.767	0.904	0.924	0.297	0.008	0.922	0.761	2.637			
		F. meli	x	all females	0.887	0.869	0.708	0.142	0.783	0.963	0.771	0.275			
		F. sicula	x	all females	0.328	0.915	0.708	0.978	0.379	0.844	0.771	0.879			
	Intra vs. Interspecific	M. meli	x	all males	0.622	0.904	0.874	0.492	0.502	0.922	0.833	0.671			
		M. sicula	x	all males	0.436	0.924	0.874	0.778	0.035	0.761	0.833	2.104			
		resBF	Between sexes	F. meli	x	M. meli	0.914	0.866	0.712	0.108	0.899	0.793	0.798	0.127	AF shape
				F. sicula	x	M. sicula	0.790	0.715	0.781	0.266	0.909	0.877	0.863	0.113	
	Between species	F. meli	x	F. sicula	0.747	0.866	0.715	0.323	0.955	0.793	0.877	0.056			
		M. meli	x	M. sicula	0.601	0.712	0.781	0.523	0.861	0.798	0.863	0.175			
		Intra vs. Interspecific	F. meli	x	all females	0.892	0.866	0.749	0.136	0.822	0.793	0.689	0.224		
			F. sicula	x	all females	0.621	0.715	0.749	0.495	0.811	0.877	0.689	0.239		
	Intra vs. Interspecific	M. meli	x	all males	0.524	0.712	0.748	0.637	0.851	0.798	0.684	0.188			
		M. sicula	x	all males	0.191	0.781	0.748	1.308	0.660	0.863	0.684	0.439			
		resMusculature	Between sexes	F. meli	x	M. meli	0.276	0.951	0.918	1.088	0.754	0.956	0.924	0.314	
				F. sicula	x	M. sicula	0.900	0.878	0.973	0.126	0.773	0.910	0.866	0.289	
	Between species	F. meli	x	F. sicula	0.703	0.951	0.878	0.381	0.224	0.956	0.910	1.216			
		M. meli	x	M. sicula	0.407	0.918	0.973	0.829	0.256	0.924	0.866	1.134			

(Continued)

Table 7. (Continued).

				Skull				Mandible				
				<i>P</i>	rPLS 1	rPLS 2	Z-score	<i>P</i>	rPLS 1	rPLS 2	Z-score	
	Intra vs. In-	F. meli	x	all fe-	0.582	0.951	0.904	0.550	0.439	0.956	0.859	0.773
	terspecific	F. sicula	x	all fe-	0.939	0.878	0.904	0.077	0.668	0.910	0.859	0.429
		M. meli	x	all males	0.964	0.918	0.877	0.046	0.799	0.924	0.844	0.254
		M. sicula	x	all males	0.342	0.973	0.877	0.950	0.177	0.866	0.844	1.349
Ecology	Between sexes	F. meli	x	M. meli	0.029	0.828	0.959	2.177	0.009	0.665	0.966	2.621
		F. sicula	x	M. sicula	0.908	0.799	0.861	0.115	0.322	0.940	0.824	0.991
	Between species	F. meli	x	F. sicula	0.617	0.828	0.799	0.500	0.055	0.665	0.940	1.921
		M. meli	x	M. sicula	0.084	0.959	0.861	1.729	0.054	0.966	0.824	1.928
	Intra vs. In-	F. meli	x	all fe-	0.049	0.828	0.898	1.966	0.075	0.665	0.793	1.783
	terspecific	F. sicula	x	all fe-	0.254	0.799	0.898	1.141	0.812	0.940	0.793	0.237
		M. meli	x	all males	0.604	0.959	0.843	0.519	0.932	0.966	0.845	0.085
		M. sicula	x	all males	0.175	0.861	0.843	1.354	0.071	0.824	0.845	1.804

Bold values indicate a significant difference between the compared rPLS.

force and morphology is explained primarily by size effects and allometry, whereas muscle forces appear to covary with shape corrected for allometry. Thus, shape variation beyond that imposed by overall size variation seems to reflect local constraints imposed by the development of more forceful jaw muscles in these lizards. We identified two types of shape variation patterns associated with variation in other traits. The first type includes covariation patterns that are functionally related to muscle packing constraints (e.g., the height of skull roof, the robustness of the coronoid process), while the second includes patterns (e.g., the height of the snout, the ventral curvature of the mandible) likely reflecting the mechanical constraints associated with the distribution of strains throughout the masticatory system. Biomechanical models aiming at understanding the functional and mechanical consequences of the observed morphological variation are needed to fully understand the observed patterns, however.

At present, we cannot demonstrate that the observed patterns are convergent at the intra- and interspecific level in this island system. This is because, to our knowledge, no reliable statistical tool exists to directly test for convergence in the association between groups of continuous multivariate traits (such as shape

and the ecological variables used in the present study; but see Bergmann and McElroy 2014 for a possible approach).

FROM MICRO TO MACROEVOLUTION IN AN ISLAND RADIATION

The comparison of the rPLS (Table 7) and the qualitative description of the evolutionary trajectories suggest that patterns of intraspecific variation are replicated at the interspecific level. In other words, we showed that under similar ecological circumstances, predictable response in musculature occurs, and that in turn, variation in muscle architecture is associated with similar patterns of morphological variation among populations and among species. Such consistency between hierarchical levels of biological integration was proposed to be the result of selection (Calsbeek et al. 2006), and likely to underlie the genesis of phenotypic diversity (Kaliontzopoulou et al. 2018). Gould (1989) proposed that evolution is the result of selection plus contingency rendering convergence less likely in more distantly related organisms. Additionally, Blount and co-authors (2018) showed that repeatable evolution of traits is more likely to occur in closely related lineages as is observed in our study comparing two species of the same genus. Put another way, the power of

selection to produce convergent phenotypes in similar ecological contexts decreases in distant taxa because of the genetic differences that accumulate over time, while the power of contingency increases. The patterns of covariation described here suggest that at least part of the hypothesis is true. Whether this can be extrapolated to the genus or even family level remains to be tested, however.

MAIN CONCLUSIONS

The relationships between head dimensions, bite force, and ecology at the interspecific level have received great attention over the past decades. The weak link between morphology and diet at the intraspecific level has been proposed to be caused by the prevalence of other agents of selection such as intraspecific competition and the need for food partitioning (Schoener 1967; Herrel et al. 1999, Vanhooydonck et al. 2010), or sexual selection through male-male combat (Sagonas et al. 2014; Lopez-Darias et al. 2015; Donihue et al. 2016). Using insular *Podarcis* lizards as a model system, we demonstrated that diet and sexual competition are both important drivers of phenotypic diversity at the intra- and interspecific level. However, phenotypic evolution is sometimes fluctuating and may only rarely be translated into long-term directional change (Gibbs and Grant 1987; Hairston and Dillon 1990; Ellner et al. 1999; Grant and Grant 2006). The present study shows that ecological pressures at the population level are strong enough to allow the emergence of macroevolutionary patterns of variation across the Adriatic thus linking population-level processes to interspecific patterns of variation.

AUTHOR CONTRIBUTIONS

A.H. designed the study. M.T., H.D., and M.F. CT-scanned the specimens. M.T. performed the statistical analyses. A.S., D.L., Z.T., and A.C.F. made the fieldwork possible and Z.T. obtained research permits for the study. A.S. generated the phylogeny. M.T. drafted the manuscript and all authors read, approved, and contributed to the final version.

ACKNOWLEDGMENTS

We would like to thank the associate editor Miriam Zelditch and the three anonymous reviewers for their very constructive and insightful comments that really helped us in improving the manuscript. We also are grateful to Antigoni Kaliontzopoulou and Fanny Pagès for their help with the comparative analyses. This project was funded by a National Geographic Explorer Grant to A.H., by a doctoral scholarship provided by Sorbonne Université (IDEX SUPER SU-17-R-DOC-03), by a travel grant provided by the doctoral school ED227 (Transhumance program) to M.T., and by a Croatian Science Foundation grant (HRZZ-IP-2016-06-9177) to A.S.

ETHICAL NOTE

Research and collecting permits were delivered by the Croatian ministry of environment and energy (permit number: 517-07-1-1-1-16-6).

DATA ARCHIVING

Data related to the present study is available online on a Dryad repository (<https://doi.org/10.5061/dryad.b5mkkwhdn>).

CONFLICT OF INTEREST

The authors declare no conflict of interest.

LITERATURE CITED

- Adams, D. C., and E. Otárola-Castillo. 2013. geomorph: an R package for the collection and analysis of geometric morphometric shape data. *Methods Ecol. Evol.* 4:393–399.
- Adams, D. C., Rohlf, F. J., and Slice, D. E. 2013. A field comes of age: geometric morphometrics in the 21st century. *Hystrix* 24(1): 7.
- Altshuler, D. L., J. W. Bahlman, R. Dakin, A. H. Gaede, B. Goller, D. Lentink, P. S. Segre, and D. A. Skandalis. 2015. The biophysics of bird flight: functional relationships integrate aerodynamics, morphology, kinematics, muscles, and sensors. *Can. J. Zool.* 93:961–975.
- Baeckens, S., and R. Van Damme. 2020. The island syndrome. *Curr. Biol.* 30:338–339.
- Barel, C. D., G. C. Anker, F. Witte, R. J. Hoogerhoud, and T. Goldschmidt. 1989. Constructional constraint and its ecomorphological implications. *Acta Morphol. Neerl. Scand.* 27:83–109.
- Bergmann, P. J., and E. J. McElroy. 2014. Many-to-many mapping of phenotype to performance: an extension of the F-matrix for studying functional complexity. *Evolutionary Biology* 41:546–560.
- Blount, Z. D., Lenski, R. E., and Losos, J. B. 2018. Contingency and determinism in evolution: Replaying life's tape. *Science* 362:6415.
- Boag, P. T., and P. R. Grant. 1981. Intense natural selection in a population of Darwin's finches (Geospizinae) in the Galapagos. *Science* 214:82–85.
- Bookstein, F. L. 1997. *Morphometric tools for landmark data: geometry and biology* Cambridge University Press.
- Calsbeek, R., J. H. Knouft, and T. B. Smith. 2006. Variation in scale numbers is consistent with ecologically based natural selection acting within and between lizard species. *Evolutionary Ecology* 20:377–394.
- Campbell-Staton, S. C., Z. A. Cheviron, N. Rochette, J. Catchen, J. B. Losos, and S. V. Edwards. 2017. Winter storms drive rapid phenotypic, regulatory, and genomic shifts in the green anole lizard. *Science* 357:495–498.
- Cardini, A. 2016. Lost in the other half: improving accuracy in geometric morphometric analyses of one side of bilaterally symmetric structures. *Syst. Biol.* 65:1096–1106.
- Cardini, A. 2017. Left, right or both? Estimating and improving accuracy of one-side-only geometric morphometric analyses of cranial variation. *Journal of Zoological Systematics and Evolutionary Research* 55:1–10.
- Cornette, R., A. Tresset, and A. Herrel. 2015. The shrew tamed by Wolff's law: Do functional constraints shape the skull through muscle and bone covariation? *J. Morphol.* 276:301–309.
- Currey, J. D. 2002. The structure of bone tissue. In: J. D. Currey, ed. *Bones: Structure and mechanics*. Princeton University Press, New Jersey, USA, 3–26.
- Cheverud, J. M. 1982. Phenotypic, genetic, and environmental morphological integration in the cranium. *Evolution* 36:499–516.
- Da Silva, F. O., A. C. Fabre, Y. Savriama, J. Ollonen, K. Mahlow, A. Herrel, J. Müller, and N. Di-Poi. 2018. The ecological origins of snakes as revealed by skull evolution. *Nat. Commun.* 9:1–11.
- D'Arcy, T. 1942. *On growth and form*. Cambridge University Press.
- Donihue, C. M., K. M. Brock, J. Fofopoulos, and A. Herrel. 2016. Feed or fight: testing the impact of food availability and intraspecific aggression on the functional ecology of an island lizard. *Functional Ecology* 30:566–575. <https://doi.org/10.1111/1365-2435.12550>

- Losos, J. B. 1990. Ecomorphology, performance capability, and scaling of West Indian *Anolis* lizards: an evolutionary analysis. *Ecological Monographs* 60:369–388.
- Losos, J. B. 2009. Lizards in an evolutionary tree. Ecology and Adaptive radiation of Anoles. University of California Press, CA.
- Losos, J. B., and R. E. Ricklefs. 2009. Adaptation and diversification on islands. *Nature* 457:830–836.
- Marroig, G., and J. M. Cheverud. 2005. Size as a line of least evolutionary resistance: diet and adaptive morphological radiation in New World Monkeys. *Evolution* 59:1128–1142.
- Martin, R. D., and C. F. Ross. 2005. The evolutionary and ecological context of primate vision. In J. Kremers, ed. *The primate visual system: A comparative approach*, John Wiley & Sons, Ltd 1–36.
- McGlothlin, J. W., M. E. Kobiela, H. V. Wright, D. L. Mahler, J. J. Kolbe, J. B. Losos, and E. D. Brodie III. 2018. Adaptive radiation along a deeply conserved genetic line of least resistance in *Anolis* lizards. *Evolution Letters* 4:310–322.
- Meiri, S. 2008. Evolution and ecology of lizard body sizes. *Global Ecol. Biogeogr.* 17:724–734.
- Mendez, J., A. Keys, J. T. Anderson, and F. Grande. 1960. Density of fat and bone mineral of the mammalian body. *Metabolism* 9:472–477.
- Novosolov, M., and Meiri, S. 2013. The effect of island type on lizard reproductive traits. *Journal of Biogeography* 40(12):2385–2395.
- Novosolov, M., Rodda, G. H., Feldman, A., Kadison, A. E., Dor, R., and Meiri, S. 2016. Power in numbers. Drivers of high population density in insular lizards. *Global Ecology and Biogeography* 25(1):87–95.
- Pigliucci, M., and J. Kaplan. 2000. The fall and rise of Dr Pangloss: adaptationism and the Spandrels paper 20 years later. *Trends Ecol. Evol.* 15:66–70.
- R Core Team. 2020. R: A language and environment for statistical computing. R Foundation for Statistical Computing, Vienna, Austria. URL: <https://www.R-project.org/>.
- Rieppel, O., and R. W. Gronowski. 1981. The loss of the lower temporal arcade in diapsid reptiles. *Zoological Journal of the Linnean Society* 72:203–217.
- Reilly, S. M., D. B. Miles, and L. D. McBrayer. 2007. The evolution of foraging mode paradigm in lizard ecology. In S. M. Reilly, L. D. McBrayer, D. B. Miles, eds. *In Lizard Ecology, The evolutionary consequences of foraging mode*, 17, Cambridge University Press.
- Renaud, S., J. C. Auffray, and S. De la Porte. 2010. Epigenetic effects on the mouse mandible: common features and discrepancies in remodelling due to muscular dystrophy and response to food consistency. *BMC Evol. Biol.* 10:28.
- Renaud, S., S. Pantalacci, and J. C. Auffray. 2011. Differential evolvability along lines of least resistance of upper and lower molars in island house mice. *PlosOne* 6:e18951.
- Rodrigues, H. G., R. Šumbera, and L. Hautier. 2015. Life in burrows channeled the morphological evolution of the skull in rodents: the case of African Mole-Rats (Bathyergidae, Rodentia). *Journal of Mammalian Evolution* 23:175–189.
- Roscito, J. G., and M. T. Rodrigues. 2010. Comparative cranial osteology of fossorial lizards from the tribe Gymnophthalmi (Squamata, Gymnophthalmidae). *J. Morphol.* 271:1352–1365.
- Sagnes, P., P. Gaudin, and B. Statzner. 1997. Shifts in morphometrics and their relation to hydrodynamic potential and habitat use during grayling ontogenesis. *J. Fish Biol.* 50:846–858.
- Sagonas, K., P. Pafilis, P. Lymberakis, C. M. Donihue, A. Herrel, and E. D. Valakos. 2014. Insularity affects head morphology, bite force and diet in a Mediterranean lizard. *Biol. J. Linn. Soc.* 112:469–484. <https://doi.org/10.1111/bij.12290>
- Schoener, T. W. 1967. The ecological significance of sexual dimorphism in size in the lizard *Anolis conspersus*. *Science* 155:474–477.
- Schlager, S. 2013. Morpho: Calculations and visualisations related to Geometric Morphometrics. R package version 0.23 3:195–220.
- Schluter, D. 1996. Adaptive radiation along genetic lines of least resistance. *Evolution* 50:1766–1774.
- Schluter, D. 2000. *The ecology of adaptive radiation*. Oxford Univ. Press, Oxford, U.K.
- Segall, M., A. Herrel, and R. Godoy-Diana. 2019. Hydrodynamics of frontal striking in aquatic snakes: drag, added mass, and the possible consequences for prey capture success. *Bioinspiration Biomimetics* 14:036005.
- Segall, M., R. Cornette, R. Godoy-Diana, and A. Herrel. 2020. Exploring the functional meaning of head shape disparity in aquatic snakes. *BioRxiv* (preprint).
- Stuart, Y. E., T. S. Campbell, P. A. Hohenlohe, R. G. Reynolds, L. J. Revell, and J. B. Losos. 2014. Rapid evolution of a native species following invasion by a congener. *Science* 346:463–466.
- Taverne, M., A. C. Fabre, N. King-Gillies, L. D. Krajnović, L. Martin, L. Michal, D. Petricioli, A. Štambuk, Z. Tadić, C. Vigliotti, et al. 2019. Diet variability among insular populations of *Podarcis* lizards reveals diverse strategies to face resource-limited environments. *Ecology and Evolution* 9:12408–12420.
- Taverne, M., N. King-Gillies, L. D. Krajnović, O. Mira, D. Petricioli, I. Sabolić, A. Štambuk, Z. Tadić, C. Vigliotti, B. A. Wehrle, et al. 2020. Proximate and ultimate drivers of variation in bite force in the insular lizards *Podarcis melisellensis* and *Podarcis sicula*. *Biol. J. Linn. Soc.* 131:88–108.
- Urošević, A., K. Ljubišavljević, D. Jelić, and A. Ivanović. 2012. Variation in the cranium shape of wall lizards (*Podarcis* spp.): effects of phylogenetic constraints, allometric constraints and ecology. *Zoology* 115:207–216.
- Vanhooydonck, B., F. B. Cruz, C. S. Abdala, D. B. Moreno Azocar, M. F. Bonino, and A. Herrel. 2010. Sex-specific evolution of bite performance in *Liolaemus* lizards (Iguania: Liolaemidae): the battle of the sexes. *Biol. J. Linn. Soc.* 101:461–475.
- Verwajen, D., R. Van Damme, and A. Herrel. 2002. Relationships between head size, bite force, prey handling efficiency and diet in two sympatric lacertid lizards. *Functional Ecology* 16:842–850.
- Wake, M. H. 2003. The skull as a locomotor organ. In J. Hanken & B. K. Hall, eds. *The skull*. University of Chicago Press.
- Wake, D. B., G. Roth. 1989. In D. B. Wake, G. Roth, eds. *Complex organismal functions: integration and evolution in vertebrates*. John Wiley & Sons, Chichester, UK.
- Witorski, A., J. B. Losos, and A. Herrel. 2016. Proximate determinants of bite force in *Anolis* lizards. *J. Anat.* 228:85–95.
- Whittaker, R. J., Fernandez-Palacios, J. M., Matthews, T. J., Borregaard, M. K., and Triantis, K. A. 2017. Island biogeography: taking the long view of nature's laboratories. *Science* 357:885.
- Zweers, G. A. 1979. Explanation of structure by optimization and systematization. *Netherlands Journal of Zoology* 29:418–440.

Associate Editor: Dr. Tiana Kohlsdorf
 Handling Editor: Dr. Miriam Zelditch

Supporting Information

Additional supporting information may be found online in the Supporting Information section at the end of the article.

Supplementary Information 1: Distribution of all the individuals included in the present study in the morphospace based on skull shape data. BD: Veli Budikovać, BM: Mali Barjak, Br: Brusnik, Bu: Veli Barjak, GL: Glavat, GR: Greben, J: Jabuka, Ko: Kopače, PG: Mala Palagruža, PK: Pod Kopače, PM: Pod Mrčaru, PZ: Mali Parzanj, Si: Sinj, St: Split, Su: Susač, T: Veli Tajana

Supplementary Information 2: Interspecific comparisons of the allometric trajectories between the PCSA of the main jaw muscle groups and skull centroid size (Csize). Represented are female individuals of *P. sicula* (in red) and of *P. melisellensis* (in black). Note that although significant, differences in allometric slopes between species are slight.

Supplementary Information 3: Contributions of the variables within each block to the axes of covariation resulting from the two-block partial least squares analyses (2b-pls)

Supplementary Information 4: Results of the intraspecific two-block partial least-squares analyses (2b-PLS) between bite force (BF), muscular data (muscle PCSA and MASS), resource use (PLANT: proportion of plants, HARD: proportion of hard prey items in the diet) at the population level

Supplementary Information 5: Results of the multiple regressions between bite force (BF), the proportion of plants (PLANT), the proportion of hard prey items (HARD), or the sexual dimorphism in head dimensions (SDh) on one hand, and the PCSA (Physiological Cross-Sectional Area), the mass and the mean fiber length of the 5 muscle groups (DM: jaw opener, ADD: external adductors, PSEU: pseudotemporalis, PTG: pterygoids, CONST: constrictor dorsalis muscles) on the other hand. s : slope, β : standardized coefficient, R^2 : coefficient of determination, P : p-value. Bold values indicate retained models. Values in blue and red indicate a negative and a positive correlation, respectively